ISSN 0915-633X

NIFS--105

JP9112194

Role of Compressibility on Driven Magnetic Reconnection

T. Sato, T. Hayashi, K. Watanabe, R. Horiuchi
M. Tanaka, N. Sawairi and K. Kusano

(Received – July 26, 1991)

NIFS-105 Aug. 1991

Role of Compressibility on Driven Magnetic Reconnection

T. Sato, T. Hayashi, K. Watanabe, R. Horiuchi, M. Tanaka
National Institute for Fusion Science
Nagoya 464, Japan

and

N. Sawairi, K. Kusano
Faculty of Science, Hiroshima University
Higashi Hiroshima 724, Japan

Abstract

Whether it is induced by an ideal (current driven) instability or by an external force, plasma flow causes a change in the magnetic field configuration and often gives rise to a current intensification locally, thereby a fast driven reconnection being driven there. Many dramatic phenomena in magnetically confined plasmas such as magnetospheric substorms, solar flares, MHD self-organization and tokamak sawtooth crash, may be attributed to this fast driven reconnection. Using a fourth order MHD simulation code it is confirmed that compressibility of the plasma plays a crucial role in leading to a fast (MHD time scale) driven reconnection. This indicates that the incompressible representation is not always applicable to the study of a global dynamical behavior of a magnetically confined plasma.

Keywords
driven magnetic reconnection, compressibility, magnetohydrodynamics, numerical simulation

1. INTRODUCTION

More than a decade has passed since the numerical demonstration that a converging flow toward a neutral sheet drives rapid magnetic reconnection.[1] This reconnection is now called "driven" reconnection and creates a Petschek type slow shock[2], whereby a rapid bulk plasma acceleration takes place. Satellite observations indicate that magnetospheric substorms, particularly large ones, occur with the delay of a few tens of minutes after the southward turning of the Interplanetary Magnetic Field (IMF) near the dayside magnetopause [3,4]. Two dimensional model simulations [5] have demonstrated that the compression of the magnetotail due to the dayside reconnection drives reconnection in the tail. Recent high resolution global simulations [6] have given, quantitatively as well as qualitatively, a reliable evidence that compression of the magnetotail by the excess flux generated by dayside reconnection with the southward IMF causes a fast reconnection in the near-earth tail and creates a developing huge plasmoid.

The previous simulation study on the fundamental process of driven magnetic reconnection already reveals that the reconnection rate is relatively independent of resistivity but strongly dependent on, say, linearly proportional to, the amplitude of the driving plasma flow [1]. This fact is not only important in explaining rapid occurrence of reconnection in the nearly collisionless magnetotail, but also has resolved a puzzing problem of magnetohydrodynamic self-organization process [7] . This problem is such that a free magnetic energy dissipates in a much faster time scale than the ohmic (resistive) dissipation time scale and that the magnetic topology changes in the same fast time scale[8]. In the MHD self-organization process an ideal MHD instability, often a current driven helical kink instability, is excited in the initial phase and the resulting plasma convection acts to deform the magnetic field configuration. At a converging point (or line) of the generated convection, driven magnetohydrodynamically is magnetic reconnection whereby magnetic topology is changed and magnetic energy is lost in a much faster time scale than the resistive diffusion .

The time scale of driven reconnection is on the order of $(V_A/V)\tau_A$, where V is the amplitude of the driving flow, V_A is the Alfven speed and τ_A is the Alfven transit time. Since V is considered to be $0.1 \sim 0.01 V_A$, this time scale is much shorter than the classical

diffusion time, τ_R , which is usually on the order of $10^6 \sim 10^{10}\tau_A$.

The most interesting and remarkable point of driven reconnection is the localized intensification of current due to the converging driving flow. Because of this local current intensification the (ohmic) electric field (reconnection rate) as well as the ohmic dissipation rate at the X (reconnection) point are greatly enhanced. This thus leads to a rapid reconnection, namely, a rapid topology change and rapid energy relaxation [8].

Recent two computer simulations of sawtooth phenomena in tokamaks, one being based on an incompressible resistive code [9] and the other based on a compressible resistive code [10], have revealed an important and suggestive difference in their results. The incompressible code has shown that the time scale of the fast crash of a sawtooth is relatively slow and strongly dependent on resistivity, while the compressible code has shown that it is fast, on the order of 100 τ_A , and rather independent of resistivity. In this regard, successful operations of JET [11] have revealed that the fast crash time scale cannot be explained by the simple Kadomtsev reconnection [12] based on a conventional resistive reconnection. This observational fact seems to favor the driven reconnection rather than the conventional resistive reconnection including the resistive tearing mode.

The very motivation of the present work emerges from this essential difference appearing in the incompressible and compressible simulations. As can be understood from the nature of driven reconnection, a great deal of current intensification is necessary for triggering it when the plasma concerned is almost collisionless. The current sheet width, d, must be compressed locally as narrow as $d \sim (V_A/VR_m)L$ where $R_m(=\tau_R/\tau_A)$ is the magnetic Raynolds number and L is the characteristic spatial scale of the initial state [8]. In reality, d can be smaller than the ion Larmor radius. Then, some microscopic instability may be excited to generate anomalous resistivity, or possibly a yet unveiled collisionless driven reconnection may be excited [13] , and the evolution of driven reconnection would be more accelerated.

As a matter of course, in a purely incompressible plasma, reconnection can be triggered only when dissipation is locally perturbed in a neutral sheet current. In other words, only dissipation-driven, or resistivity-driven reconnection is possible. The necessity of drastic local current intensification therefore requires that plasma be compressible. We thus wish to clarify the role of compressibility on driven reconnection in this work. For this purpose

we rely on a simulation and use a two dimensional compressible, resistive MHD code with the fourth order accuracy both in space and time.

2. SIMULATION MODEL

We adopt a simulation model similar to the previous one [1]. However, we employ a more reliable simulation code which adopts the fourth order difference for the spatial derivative and the fourth order Range-Kutta-Gill scheme for time advancing[14]. The simulation box is assigned much larger and the resistivity is assumed to be uniform and constant rather than nonlinear [1].

The governing equations are the conventional MHD equations as follows:

$$\frac{\partial \rho}{\partial t} + \nabla \cdot (\rho \boldsymbol{v}) = 0 \tag{1}$$

$$\rho \frac{d \boldsymbol{v}}{d t} = \boldsymbol{J} \times \boldsymbol{B} - \nabla p \tag{2}$$

$$\frac{\partial \boldsymbol{B}}{\partial t} = \nabla \times (\boldsymbol{v} \times \boldsymbol{B}) - \nabla \times (\eta \boldsymbol{J}) \tag{3}$$

$$\frac{\partial p}{\partial t} + \nabla \cdot (p \boldsymbol{v}) = (\gamma - 1)(-p \nabla \cdot \boldsymbol{v} + \eta \boldsymbol{J}^2) \tag{4}$$

where the notation is conventional; $\mu_0 \boldsymbol{J} = \nabla \times \boldsymbol{B}$, η is the resistivity, γ is the adiabatic constant and μ_0 is the permeability.

The simulation box is a rectangular box in the $x - z$ plane in which a Harris type equilibrium (suffix 0 is attached) is given:

$$B_{z0}(x) = \tanh x \tag{5}$$

$$P_0(x) = \mathrm{sech}^2 x + P \tag{6}$$

$$J_{y0}(x) = \mathrm{sech}^2 x \tag{7}$$

$$B_{y0}(x) = B_y \tag{8}$$

where B_y and P are constant.

We assume that driving plasma flow flows into the simulation box symmetrically from the two input boundaries placed at $x = x_0$ and $x = -x_0$ toward the neutral sheet ($x = 0$). The flow pattern is such that it is symmetric around $z = 0$, peaked at $z = 0$ and decreasing

away from $z = 0$. In the actual simulation, the plasma inflow is driven by the electric field imposed in the y direction at the input boundary. The virtual (physical) boundaries are assumed at $z = \pm z_0$ at which plasma can freely flow in and out, namely, free physical boundaries. To realize such free boundary conditions, we add extra regions (extra meshes) outside the virtual (physical) free boundaries. The extra regions extend from $z = \pm z_0$ to $z = \pm(z_0+\delta)$. In these extra regions all perturbations are so programmed that they suffer from heavy frictional damping, specifically, a frictional force, - $\nu(z)(f-f_0)$, is added on the right hand side of each evolutional equation of Eqs. (1) - (4) where f stands for either ρ, $\boldsymbol{v}$, p or $\boldsymbol{B}$. The friction coefficient $\nu(z)$ takes on the form $\nu(z) = \nu_0\{1-\cos\pi(\mid z \mid -z_0)/2\delta\}$ for $\mid z \mid \geqq z_0$. ν_0 is fixed to 1.5 in the present runs. At $z = \pm(z+\delta)$ all derivatives are assumed to vanish.

The question is now how to change the degree of compressibility of the plasma in the MHD equations given in eqs. (1)-(4). In the present study we consider the following three cases. In the first we attempt to model the degree of compressibility by changing the value of the adiabatic constant γ with $B_y = P = 0$. Namely, we regard the plasma more incompressible when γ is much larger than unity, while more compressible when γ is closer to zero. Secondly, we attempt to model the degree of compressibility by adding the vertical (toroidal) magnetic field B_y given in eq.(8). It is not so sure whether the addition of B_y can well model the degree of compressibility or not. But one conventionally takes an incompressible representation for the tokamak plasma simply because a large external toroidal field exists and reconnection is expected to take place in the poloidal plane. The reason is that because of the large toroidal field the magnetosonic speed is supposed to be extremely large compared with the plasma flow. Thirdly, we add a constant pressure P on top of the Harris distribution. This is done only to compare the result with that of the second case.

3. TEST OF RELIABILITY OF THE FOURTH ORDER CODE

Before going into the description of the simulation runs on the role of compressibility, let us at first confirm the reliability of the fourth order code.

We have done simulations for completely the same conditions as the previous ones [1].

The comparison is shown in Figs. 1 and 2. The overall development behaviors of the electric field at the X point, the reconnection rate, are in fairly good agreement with each other. Specifically, the reconnection rate is only slightly dependent on resistivity, while it is linearly proportional to the driving flow speed.

One can notice, however, that the present code gives a much finer structure than the two-step Lax-Wendroff code. In particular, the periodic spiky structures, representing the arrivals of the magnetosonic signature at the X point as a result of bouncing between the inflow boundary ($x = x_0$) and the X point ($x = 0$), are much more clear-cut for the present simulation. This ensures that the present fourth order code presents a much more reliable result, especially for a small scale feature.

4. RESULTS OF SIMULATION

With the aim of avoiding as much an undesired effect of the boundary as possible we have adopted a much larger simulation box than the previous one : $x_0 = 3$, $z_0 = 10$ and $\delta = 3$. Furthermore, the electric field $E(z,t)$ imposed at the input boundary ($x = \bar{x}$) is programmed in the following way:

For $t \leqq t_1$,

$$E(z,t) = \begin{cases} \frac{E_0}{2}\left\{1 - \cos(\frac{|z| - V_0 t}{V_0 t_1})\pi\right\}, & |z| \leqq V_0 t \\ 0, & |z| \geqq V_0 t \end{cases} \tag{9}$$

For $t \geqq t_1$,

$$E(z,t) = \begin{cases} E_0, & |z| \leqq V_0(t - t_1) \\ \frac{E_0}{2}\left\{1 - \cos(\frac{|z| - V_0 t}{V_0 t_1})\pi\right\}, & V_0(t - t_1) \leqq |z| \leqq V_0 t \\ 0, & |z| \geqq V_0 t \end{cases} \tag{10}$$

where $t_1 = 3$ and $V_0 \cong 0.1$. The reason of taking this spatially spreading inflow pattern rather than a spatially fixed pattern is two-fold: They are to avoid a too much localized bending of the magnetic field near the input boundary and to avoid a spiky compression at the X point by letting the driving flow soft-land. The choice of constant resistivity in the present study may also contribute to softening the evolution of reconnection.

From the symmetry condition with respect to $x = 0$ and $z = 0$, the actual simulation

is done for a quarter region, $0 \leqq x \leqq 3$ and $0 \leqq z \leqq 13$. This quarter box is nested by equally spaced 200 x 300 grid points.

In order to check that the size of the simulation box in the z direction does not affect the simulation result, or the output boundary condition at $10 \leqq z \leqq 13$ does not influence upon the result, we have performed a simulation where the simulation length in the z direction is doubled, namely, $0 \leqq z \leqq 26$. Figure 3 shows the temporal evolutions of the reconnection rate for two cases. The comparison indicates that there exists no apparent difference, thus concluding that the choice of $0 \leqq z \leqq 13$ is good enough.

4.1 Representative Run

As a typical example that provides a reference run among others which represent different degrees of compressibility, we give the result of simulation where $E_0 = 0.03$, $\eta = 0.005$, $\gamma = 2$, and $B_y = P = 0$.

Figures 4 and 5 show the temporal evolutions of the magnetic field lines and the plasma flows in the entire physical region. Also shown in Fig 6 a,b are the evolutions of the contour maps of the pressure and the temperature. Formation of two-sheet slow shocks and strong acceleration at the shocks are essentially the same as the previous results [1]. A three dimensional view of the temporal evolution of the plasma current shown in Fig. 7 provides us with a very clear-cut and attractive feature of the birth of a large scale X-shape slow shock, along with remarkable current intensification at the converging (X) point of the driving flows. There will be no doubt that the observed reconnection is forced by strong compression of the plasma at the X point due to the converging flow.

4.2 Driven Flow versus Resistivity

For the present large simulation run with a constant resistivity and a spatially-expanding driving inflow we examine the difference in the influence of the strength of the driving flow and of the resistivity.

Fig. 8 a,b shows (a) the temporal evolutions of the reconnection rate (the X point electric field) for three different driving flows with a fixed resistivity, i.e., $E_0 = 0.02$, 0.03 and 0.04 for $\eta = 0.005$, and (b) those for three different resistivities with a fixed driving flow, i.e., $\eta = 0.003$, 0.005 and 0.01 for $E_0 = 0.05$. As one sees, these results recon-

firm that the evolution of reconenection (speed of evolution and saturation amplitude) has a strong relationship, almost linear relationship, with the amplitude of the driving converging flow, while a weak dependence on resistivity. Note that E_{R0} in this figure represents the initial electric field given by ηJ_0. There appears a slight difference in the evolutional behavior depending on the difference in the resistivity as shown in Fig. 8b. It is likely, however, that the difference in the resistivity influences upon the degree of compression at the X point which in turn leads to the difference in the development of driven reconnection. This is particularly so when the normalized η, namely, R_m, is closer to the normalized driving force E_0. In the present case the normalized η/E_0 is $0.3 \sim 0.1$ for $\eta = 0.01 \sim 0.03$, which is rather close to 1. It is expected therefore that the resistivity influences upon the evolution of driven reconnection. In reality, η is on the order of 10^{-6} or even smaller, so that the influence of the resistivity upon driven reconnection may be negligibly small.

4.3 Influence of Compressibility

Simulation runs have been performed for three different cases to clarify the influence of compressibility on flow driven reconnection. The first one is the case where the value of the adiabatic constant γ is changed. The second is the case where a vertical magnetic field B_{y0} is applied, and the third is the case where a uniform pressure P is applied. We shall see the results in this order.

Dependence on Adiabatic Constant

The reasonable choice of γ may be in the range between 1.5 and 3.0. However, such a small range may not be large enough to exhibit a significant difference in the evolution of driven reconnection, because the change of the magnetosonic speed can be about 20 % . We therefore change γ in an artificial way from $\gamma = 1.1 \sim 10$ to magnify the influence.

Results are shown in Figs. 9 and 10. As expected, the activity of driven reconnection is enhanced as γ approaches 1. Noted particularly is a drastic activation seen for $\gamma = 1.1$, the peak value significantly exceeding the driving electric field ($E_0 = 1.13$), when the compressibility is extremely enhanced. This feature seems to be understood by the fact that the relative role of the thermal energy increases inversely proportional to ($\gamma - 1$).

For reference, three dimensional views of the current layers are given in Fig. 10.

Dependence on Vertical Magnetic Field

It is expected that the inclusion of a vertical magnetic field would reduce the compressibility of the plasma. Figure 11a shows the evolutions of the reconnection rate for $B_y = 0$, 2 and 5. It is interesting to observe that there is no significant change for $B_y \leqq 2$. However, when $B_y = 5$, the evolution is significantly slowed down and the peak reconnection rate stays considerably below the driving rate and retained to about two-third of it. This indicates that the vertical magnetic field acts to weaker the activity of driven reconnection. In tokamaks where the ratio of the toroidal field to the poloidal one is 5 or so, therefore, it is expected that the activity of driven reconnection would be weakened to some extent. Nonetheless, it is not negligibly small.

The present result is important in the sense that the conventional incompressible representation is not good enough for the study of tokamaks, particularly when an ideal helical kink instability or another can be excited, such as the study of sawtooth phenomena and of major disruptions.

Dependence on Constant Pressure

Behaviors of driven reconnection are also studied by applying different uniform pressures P. Results for $P = 0$, 4 and 25 are shown in Fig 11b. Though not so conspicuous, a tendency is observed that the activity is slightly depressed as P increases.

5. CONCLUSIONS

In nature there are a number of attractive phenomena arising from the interaction of a plasma flow with the magnetic field. As such, we know the accreting plasma-magnetic star interaction and the solar wind-magnetosphere interaction. In magnetic confinement devices, as well, there are a number of interesting phenomena arising from the interaction of a plasma flow induced spontaneously or externally with the magnetic field. As such, we know the magnetohydrodynamic self-organization process and the magnetohydrodynamic disruption.

One common feature of those phenomena is that magnetic topology is changed locally or globally. Associated with are plasma acceleration, plasma heating and/or bulk plasma transport.

In those phenomena it is often the case that a plasma flow is the primary cause. Since the plasma of our concern is usually nearly collision-free, the flow gives rise to a change in the magnetic field configuration, whereby often a current intensification occurs locally. In nature the flow energy can be larger than the magnetic energy. In magnetic confinement devices, the plasma current is a major agency of free energy, so that it can happen that one or ten percent of the free energy is released to the plasma flow. Therefore, the maximum flow speed is likely to amount to a few percent of the Alfven speed defined by the current-induced magnetic field (self-field). The flow speed is big enough to appreciably change the self-field (poloidal field in tokamaks) configuration. One can say therefore that both in nature and in laboratory it is very likely that flow-driven reconnection takes place.

The present work has proved that the compressibility certainly plays a key role in driven reconnection. In a magnetic configuration where an externally generated large magnetic field (say, a toroidal field) exists perpendicularly to a plane in which a current-induced self field (say, a poloidal field) exists, it is found that driven reconnection is less activated. However, it does occur because of inevitably existing compressibility. This indicates that the incompressible treatment such as using a reduced set of equations may lose some crucial effects when one wishes to study a magnetohydrodynamic behavior of a magnetically confined plasma such as tokamaks, RFP and compact toroids.

Finally, let us note that a very clear, large scale current layer (slow shock) structure is realized for a constant resistivity model, as was observed for a nonlinear resistivity model [1]. Near the X point a remarkable intensification of current occurs. Toward the downstream an X shape, narrow current layer extends from the peaked current layer near the X point. Further downstream, the X shape bends and turns into a U shape. For a constant resistivity model, as well, it is reconfirmed that development of driven reconnection is rather independent of resistivity but strongly (linearly) dependent on the driving flow.

1. T. Sato and T. Hayashi, Phys. Fluids **22**, 1189 (1979); T. Hayashi and T. Sato, J. Geophys. Res., **83**, 217 (1978).
2. H.E. Petschek, NASA Spec. Pub. SP-50, 425 (1964).
3. D.N. Baker, R.D. Zwickl, S.J. Bame, E.W. Jones, Jr., B.T. Tsurutani, and E.J. Smith, J. Geophys. Res. **88**, 6230 (1983).
4. A. Nishida, *Geomagnetic Diagnostics of the Magnetosphere*, Springer-Verlag (1978).
5. K.W. Min, H. Okuda, and T. Sato, J. Geophys. Res. **90**, 4035 (1985).
6. A. Kageyama, K. Watanabe, and T. Sato, to appear in J. Geophys. Res.; A. Usadi, A. Kageyama, K. Watanabe, and T. Sato, submitted for J. Geophys. Res.
7. R. Horiuchi and T. Sato, Phys. Fluids **29**, 1161 (1986); K. Kusano and T. Sato, Nucl. Fusion **27**, 821 (1987).
8. T. Sato, R. Horiuchi, and K. Kusano, Phys. Fluids **B1**, 255 (1989).
9. A.Y. Aydemir, J.C. Wiley, and D.W. Ross, Phys. Fluids **B1**, 774 (1989).
10. T Sato, Y. Nakayama, T. Hayashi, K. Watanabe, and R. Horiuchi, Phys. Rev. Lett. **63**, 528 (1989).
11. D.T. Campbell et al., Nucl. Fusion **26**, 1085 (1986).
12. B.B. Kadomtsev, Sov. J. Plasma Phys. **1**, 389 (1975).
13. B. Coppi, Proceedings of the 2nd International Toki Conference on Plasma Physics and Controlled Nuclear Fusion: Nonlinear Phenomena in Fusion Plasmas -Theory and Computer Simulation, NIFS-PROC-6, 3 (1991).
14. R. Horiuchi and T. Sato, Phys. Fluids **B1**, 581 (1989); K. Watanabe and T. Sato, J. Geophys. Res. **95**, 75 (1990).

Figure captions

Fig. 1. Comparisons between the fourth order simulation code (present work) and the second order code (Ref. 1). The top panel is the result of the fourth order code and the bottom is that of the second order code, where temporal evolutions of the X point electric field for four different driving flows (E_0) with a fixed resistivity (α) are shown. The resistivity takes the form of $\alpha(J - J_0)^2$.

Fig. 2. Same figure as Fig. 1 for three different resistivities (α) with a fixed driving electric field E_0.

Fig. 3. The temporal evolution of the electric field at the reconnection point for the cases where the sizes of the simulation box in the z direction are equal to 13 and 26. This ensures that the box size of z = 13 is good enough.

Fig. 4. Evoulutions of the magnetic field lines in the entire physical region for the case where $E_0 = 0.03$, $\eta = 0.005$, $\gamma = 2$, and $B_y = P = 0$.

Fig. 5. Evolutions of the plasma flow vectors in the entire physical region for the same case as Fig. 4.

Fig. 6. Evolutions of the contour maps of (a) the pressure and (b) the temperature in the entire physical region for the same case as Fig. 4.

Fig. 7. Three dimensional display of the temporal evolution of the plasma current in the entire physical region for the same case as Fig. 4.

Fig. 8. (a) Temporal evolutions of the electric field at the reconnection point for three different driving flows with a fixed resistivity, i.e., $E_0 = 0.02$, 0.03, and 0.04 for $\eta = 0.005$, (b) those for three different resistivities with a fixed driving flow, i.e., $\eta = 0.003$, 0.005, and 0.01 for $E_0 = 0.05$.

Fig. 9. Temporal evolutions of the X-point electric field for the cases with four different adiabatic constants where the solid lines show the results for $\gamma = 1.1$, 2.0, 5.0, and 10.0, respectively.

Fig. 10. Three dimensional displays of the spatial profile of the plasma current at $t = 50\tau_A$ for the cases of $\gamma = 1.1$ (top), 2.0 (middle) and 10.0 (bottom).

Fig. 11. (a) Temporal evolutions of the X-point electric field for three different vertical magnetic fields, i.e., $B_y = 0,\ 2$, and 5, (b) those for three different uniform pressures, i.e., $P = 0,\ 4$, and 25.

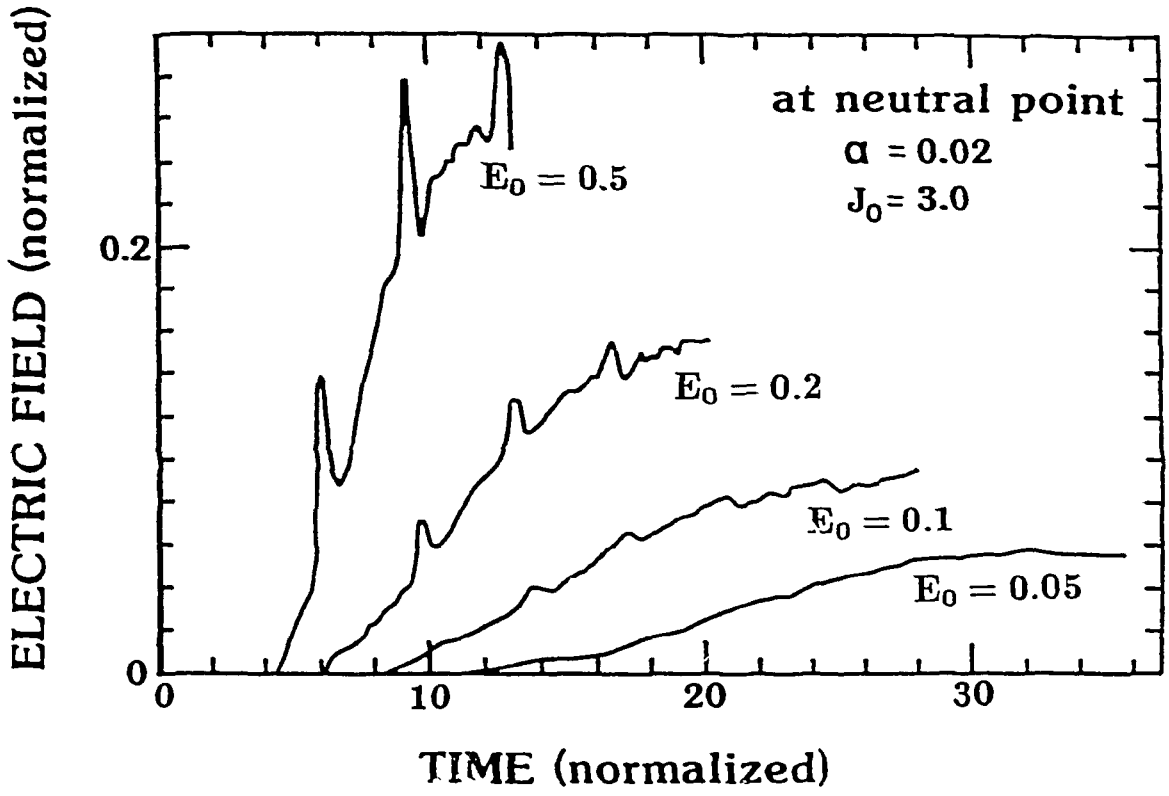
ELECTRIC FIELD (normalized)
at neutral point
α = 0.02
J0 = 3.0
E0 = 0.5
E0 = 0.2
E0 = 0.1
E0 = 0.05
0.2
0
0
10
20
30
TIME (normalized)

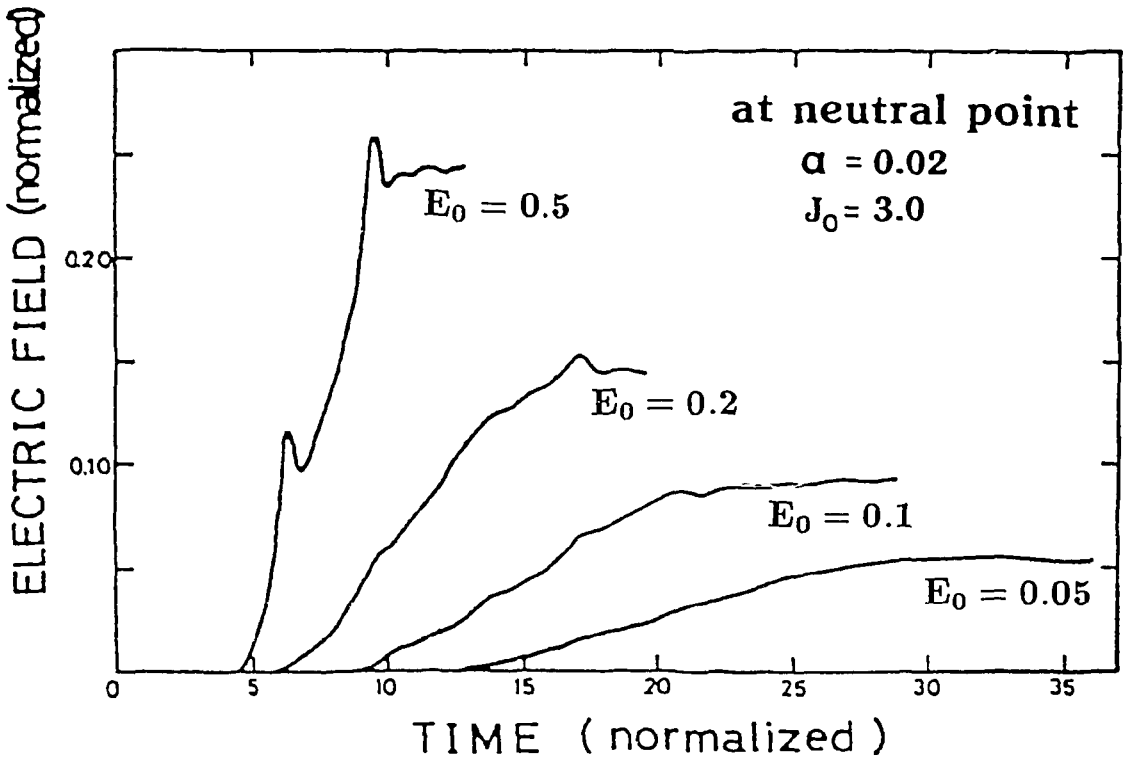
ELECTRIC FIELD (normalized)
at neutral point
α = 0.02
J0 = 3.0
E0 = 0.5
E0 = 0.2
E0 = 0.1
E0 = 0.05
0.20
0.10
0
5
10
15
20
25
30
35
TIME (normalized)

Figure 1

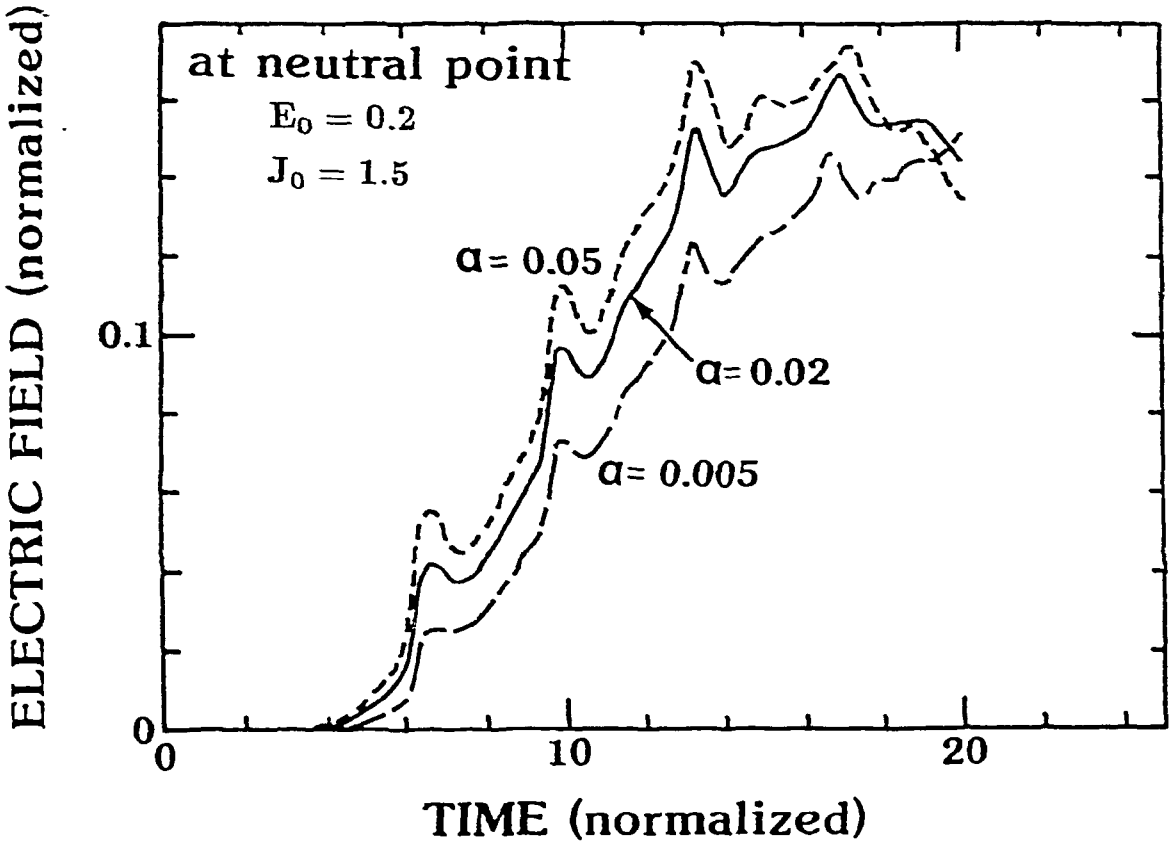
at neutral point
$E_0 = 0.2$
$J_0 = 1.5$
α= 0.05
α= 0.02
α= 0.005
ELECTRIC FIELD (normalized)
0.1
0
0
10
20
TIME (normalized)

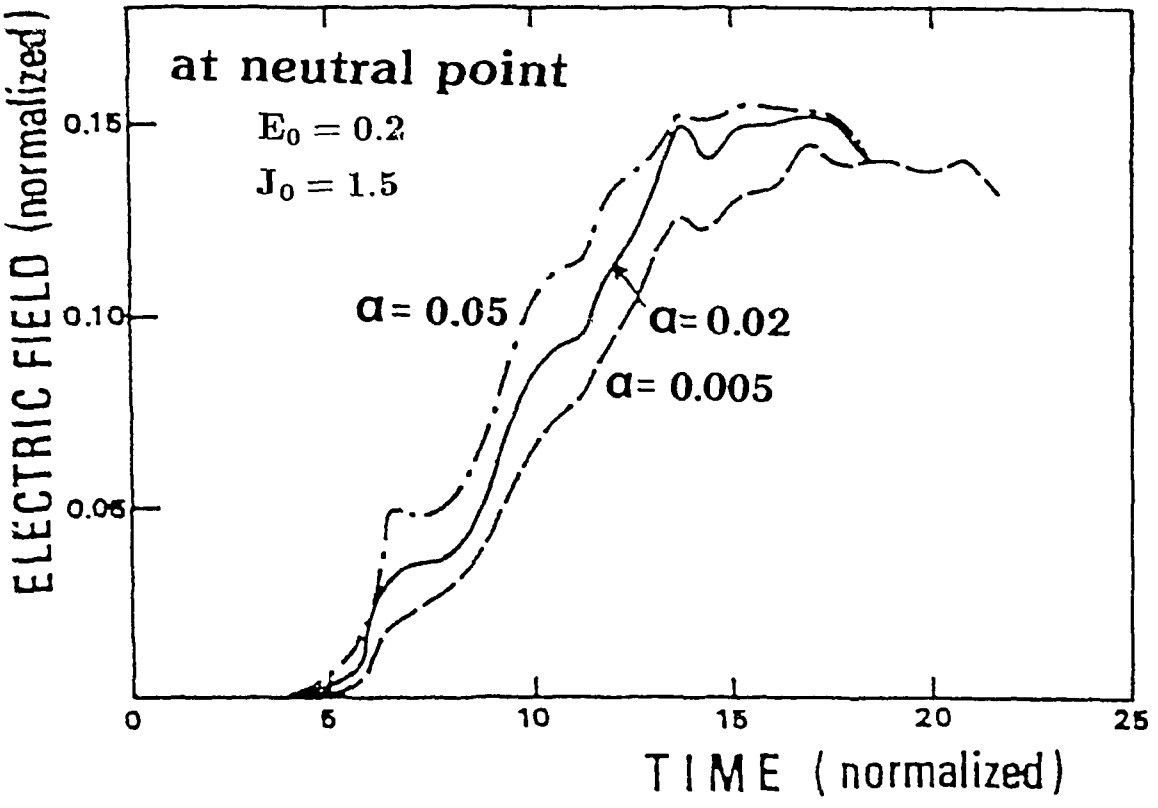
at neutral point
$E_0 = 0.2$
$J_0 = 1.5$
α= 0.05
α= 0.02
α= 0.005
ELECTRIC FIELD (normalized)
0.15
0.10
0.05
0
5
10
15
20
25
TIME (normalized)

Figure 2

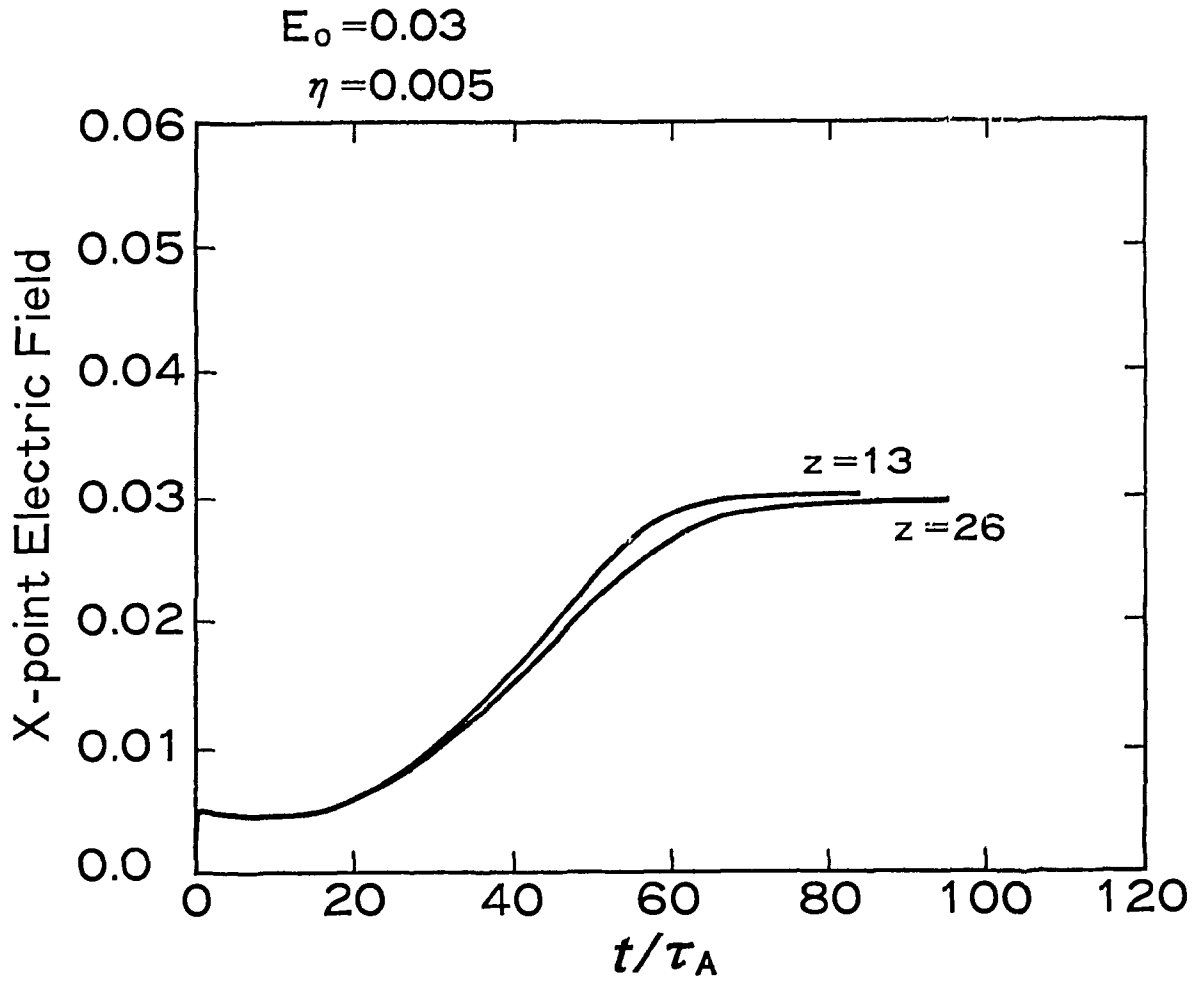
E_o=0.03
η=0.005
0.06
0.05
0.04
0.03
0.02
0.01
0.0
X-point Electric Field
z=13
z=26
0
20
40
60
80
100
120
t/τ_A

Figure 3

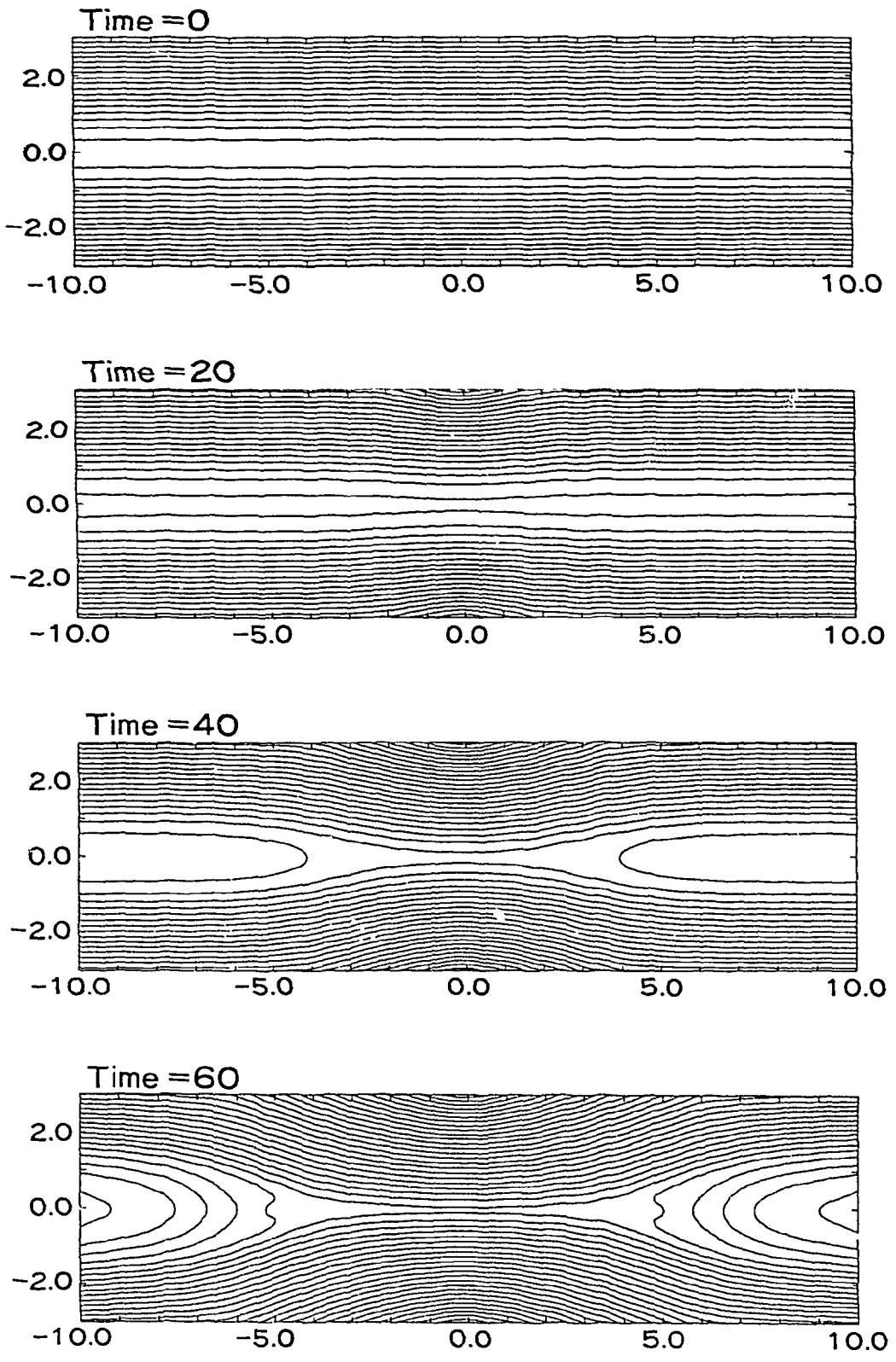
Time =0
2.0
0.0
-2.0
-10.0
-5.0
0.0
5.0
10.0
Time =20
2.0
0.0
-2.0
-10.0
-5.0
0.0
5.0
10.0
Time =40
2.0
0.0
-2.0
-10.0
-5.0
0.0
5.0
10.0
Time =60
2.0
0.0
-2.0
-10.0
-5.0
0.0
5.0
10.0

Figure 4

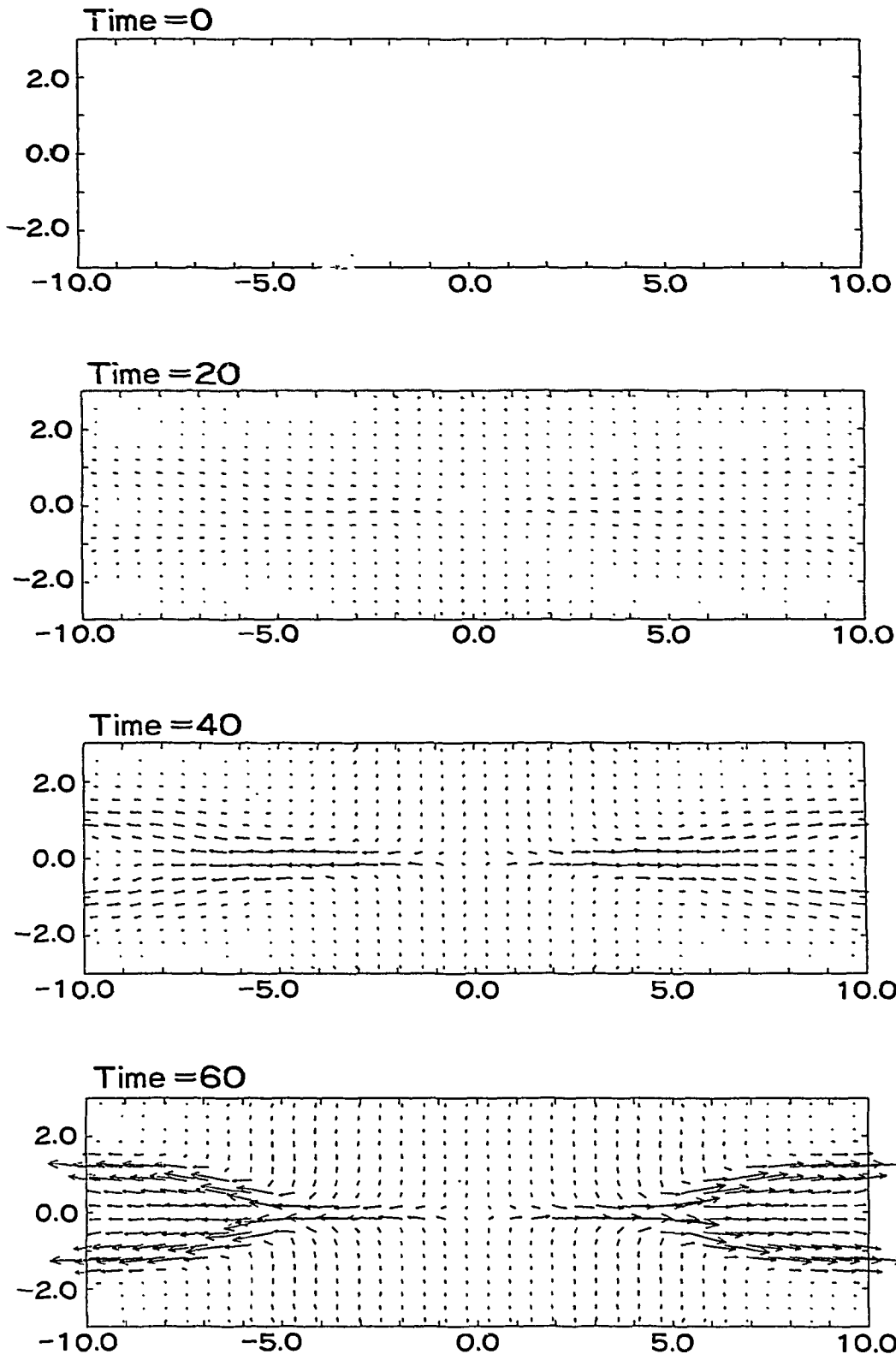
Time =0
2.0
0.0
-2.0
-10.0
-5.0
0.0
5.0
10.0
Time =20
2.0
0.0
-2.0
-10.0
-5.0
0.0
5.0
10.0
Time =40
2.0
0.0
-2.0
-10.0
-5.0
0.0
5.0
10.0
Time =60
2.0
0.0
-2.0
-10.0
-5.0
0.0
5.0
10.0

Figure 5

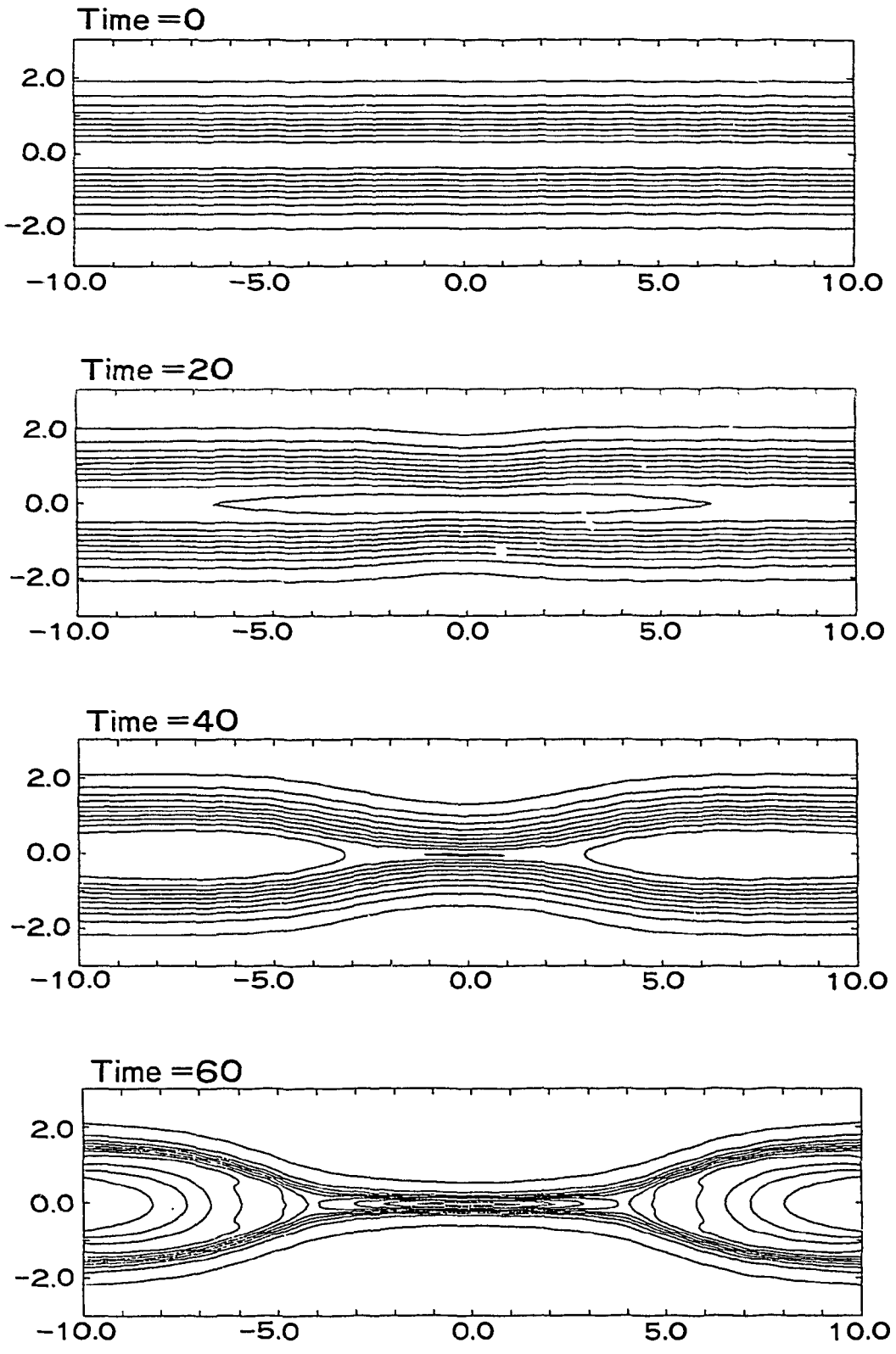
Time =0
2.0
0.0
-2.0
-10.0
-5.0
0.0
5.0
10.0
Time =20
2.0
0.0
-2.0
-10.0
-5.0
0.0
5.0
10.0
Time =40
2.0
0.0
-2.0
-10.0
-5.0
0.0
5.0
10.0
Time =60
2.0
0.0
-2.0
-10.0
-5.0
0.0
5.0
10.0

Figure 6-(a)

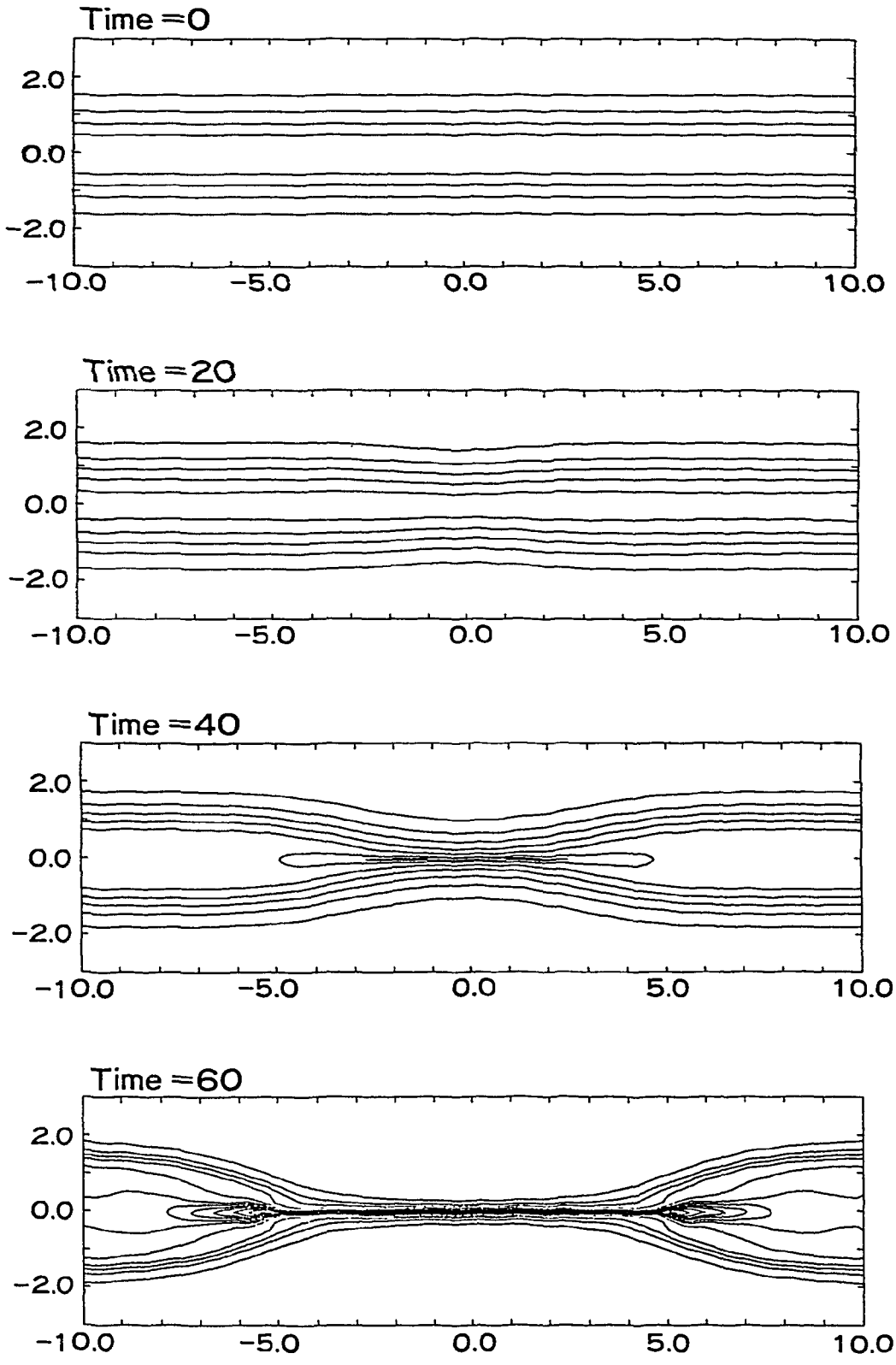
Time =0
2.0
0.0
-2.0
-10.0
-5.0
0.0
5.0
10.0
Time =20
2.0
0.0
-2.0
-10.0
-5.0
0.0
5.0
10.0
Time =40
2.0
0.0
-2.0
-10.0
-5.0
0.0
5.0
10.0
Time =60
2.0
0.0
-2.0
-10.0
-5.0
0.0
5.0
10.0

Figure 6-(b)

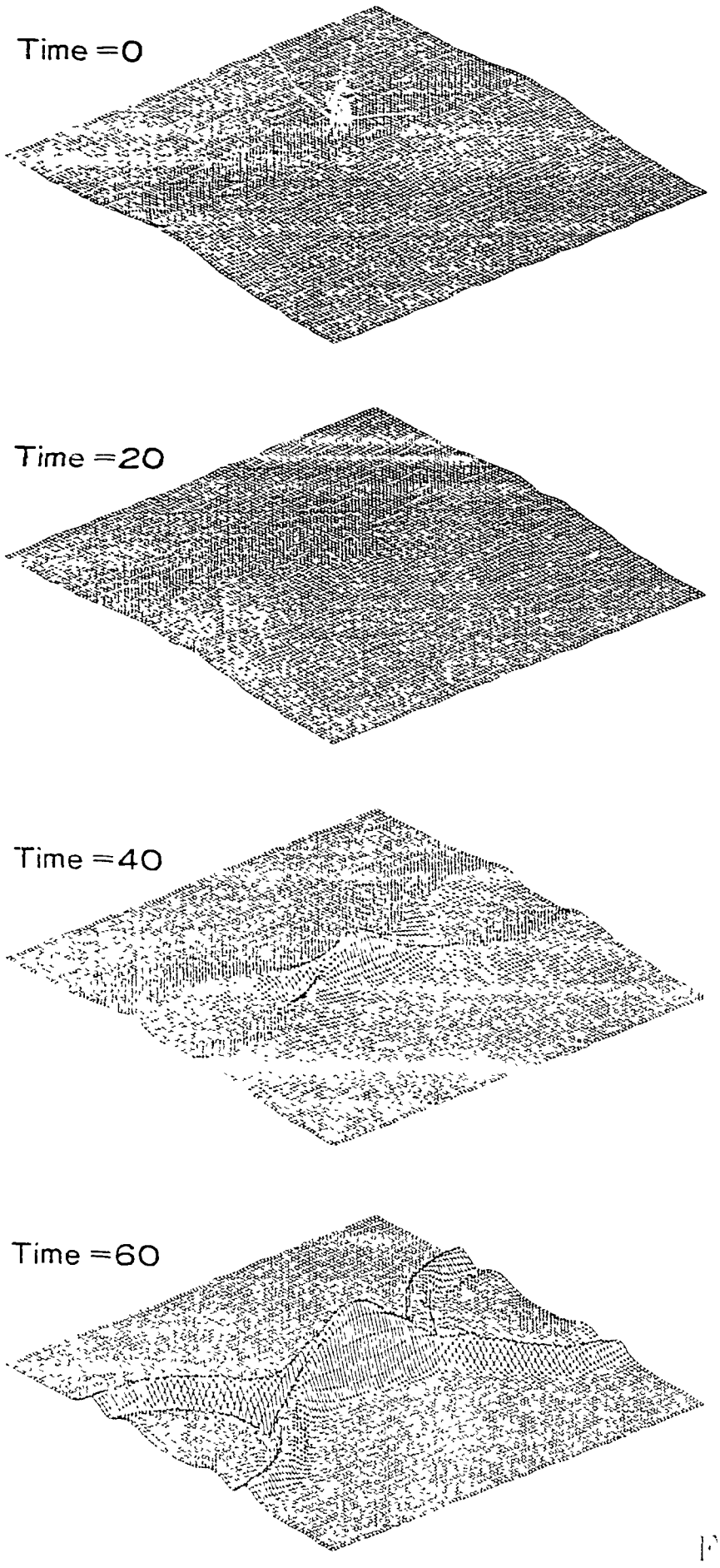

Figure 7

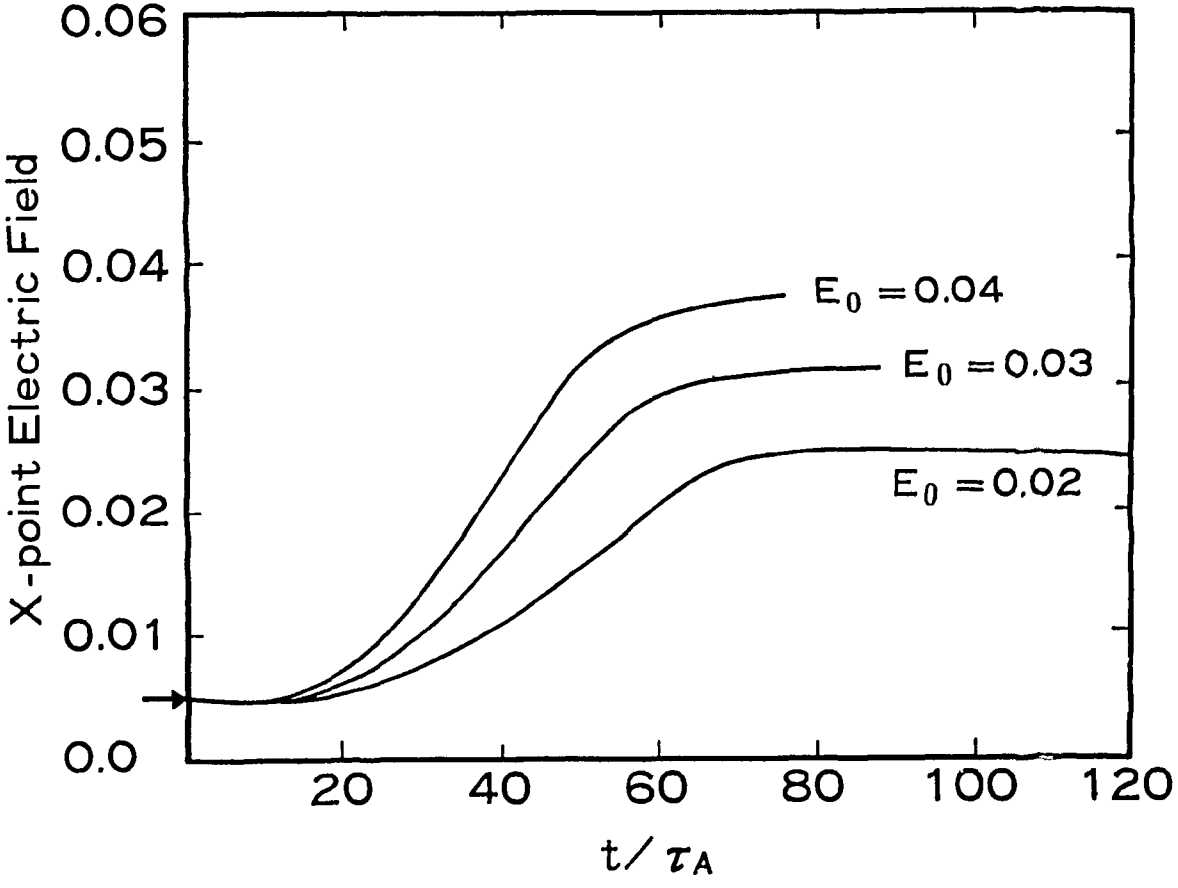
0.06
0.05
0.04
0.03
0.02
0.01
0.0
X-point Electric Field
$E_0 = 0.04$
$E_0 = 0.03$
$E_0 = 0.02$
20
40
60
80
100
120
t/τ_A

Figure 8-(a)

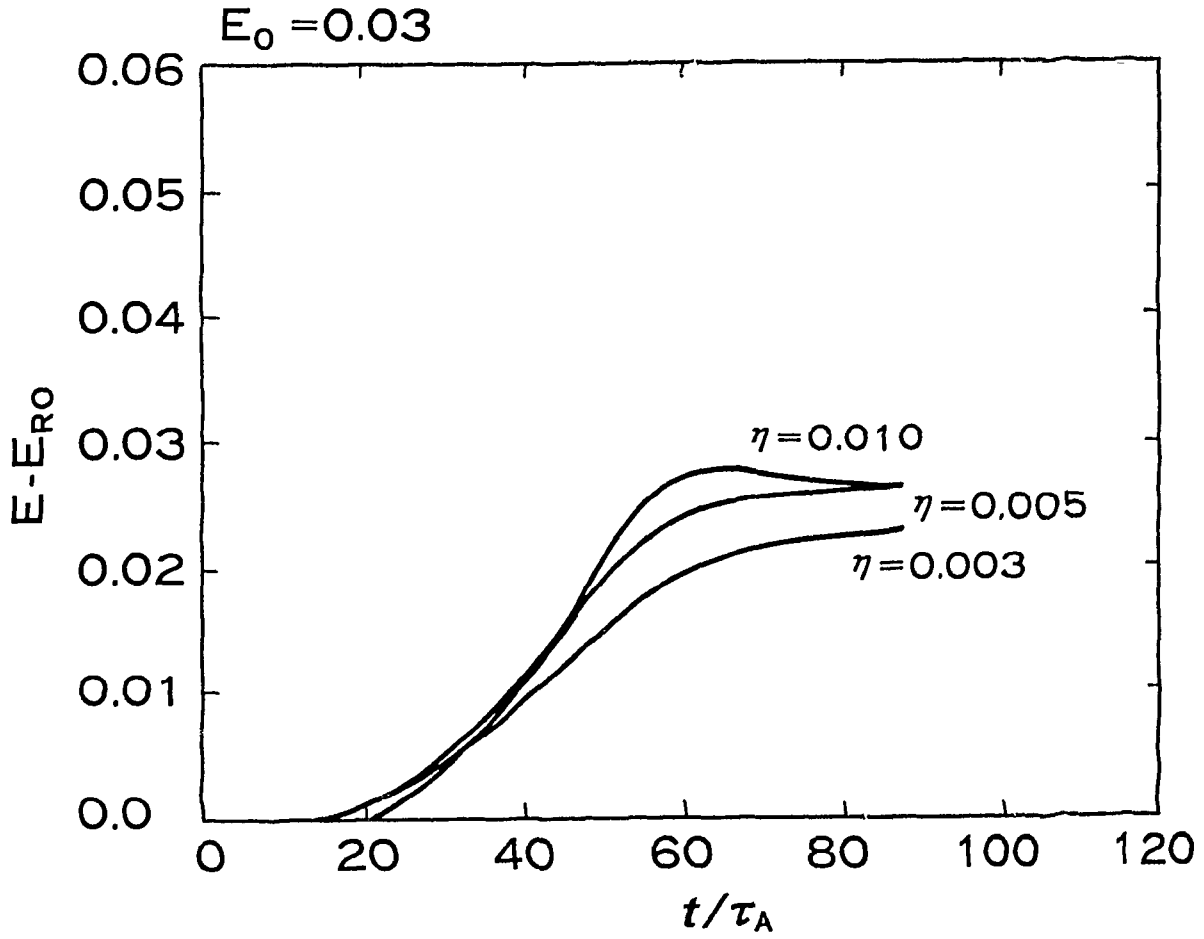
E_0 =0.03
0.06
0.05
0.04
0.03
0.02
0.01
0.0
E-E_{R0}
η=0.010
η=0.005
η=0.003
0
20
40
60
80
100
120
t/τ_A

Figure 8-(b)

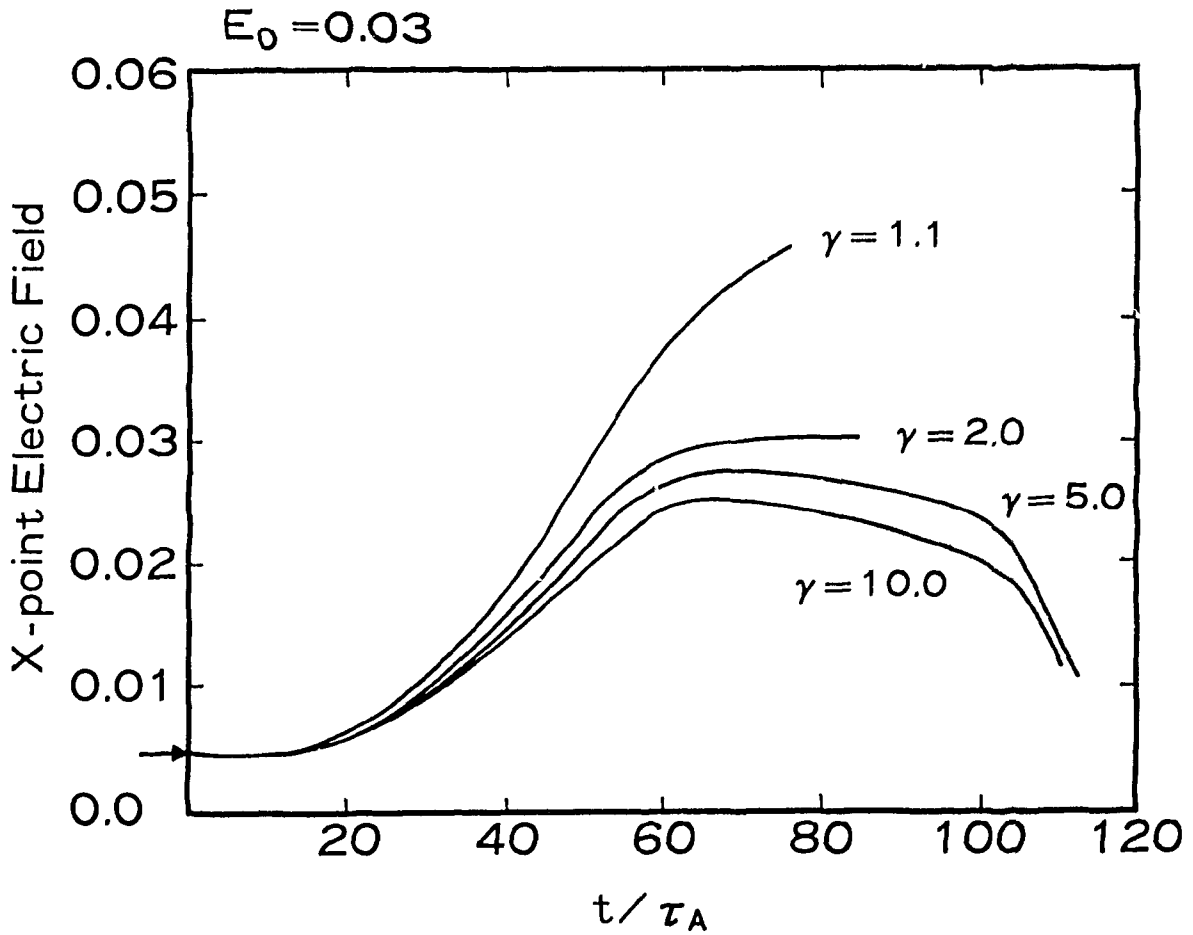
$E_0 = 0.03$
0.06
0.05
0.04
0.03
0.02
0.01
0.0
X-point Electric Field
$\gamma = 1.1$
$\gamma = 2.0$
$\gamma = 5.0$
$\gamma = 10.0$
20
40
60
80
100
120
t/τ_A

Figure 9

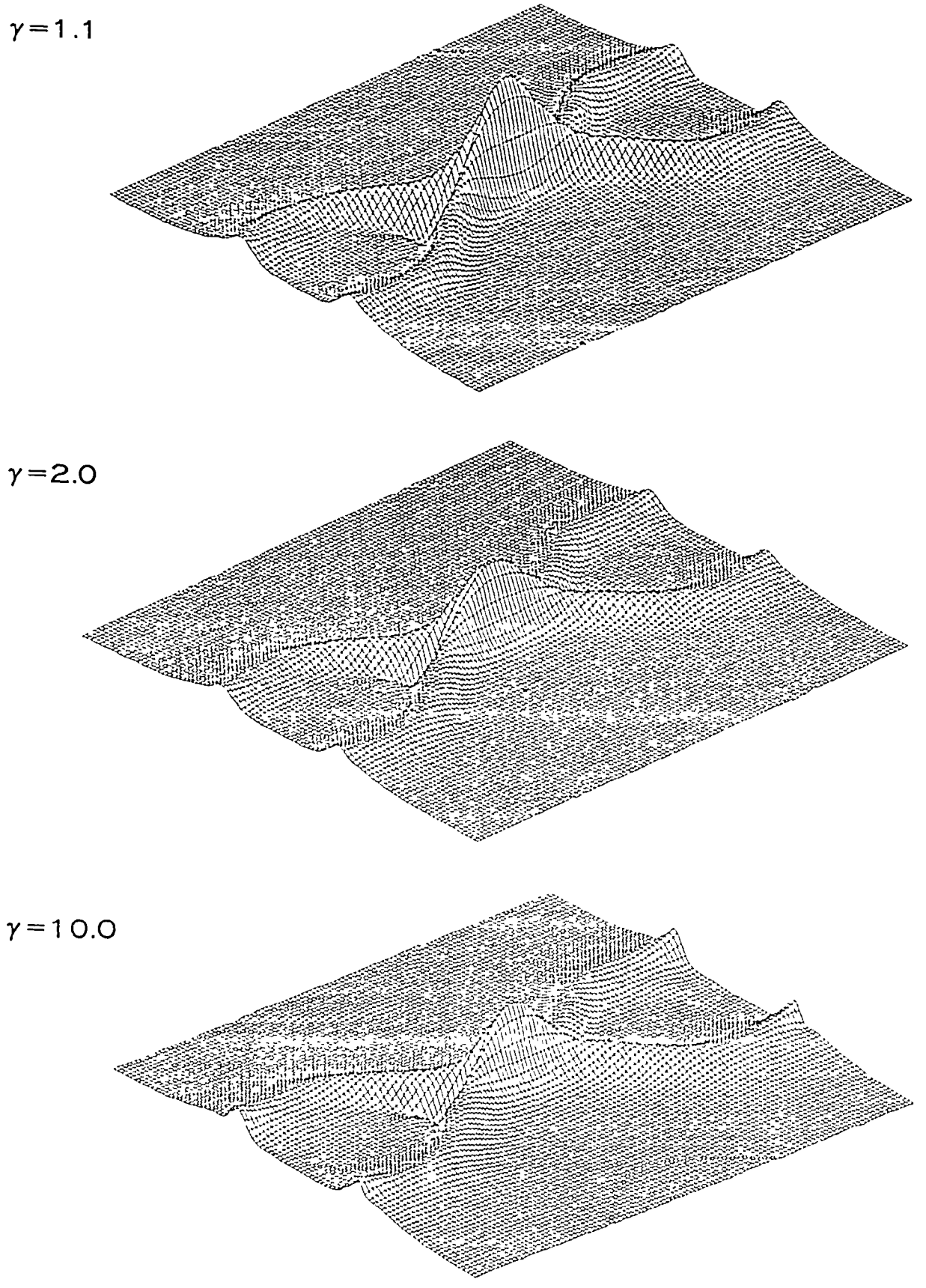

Figure 10

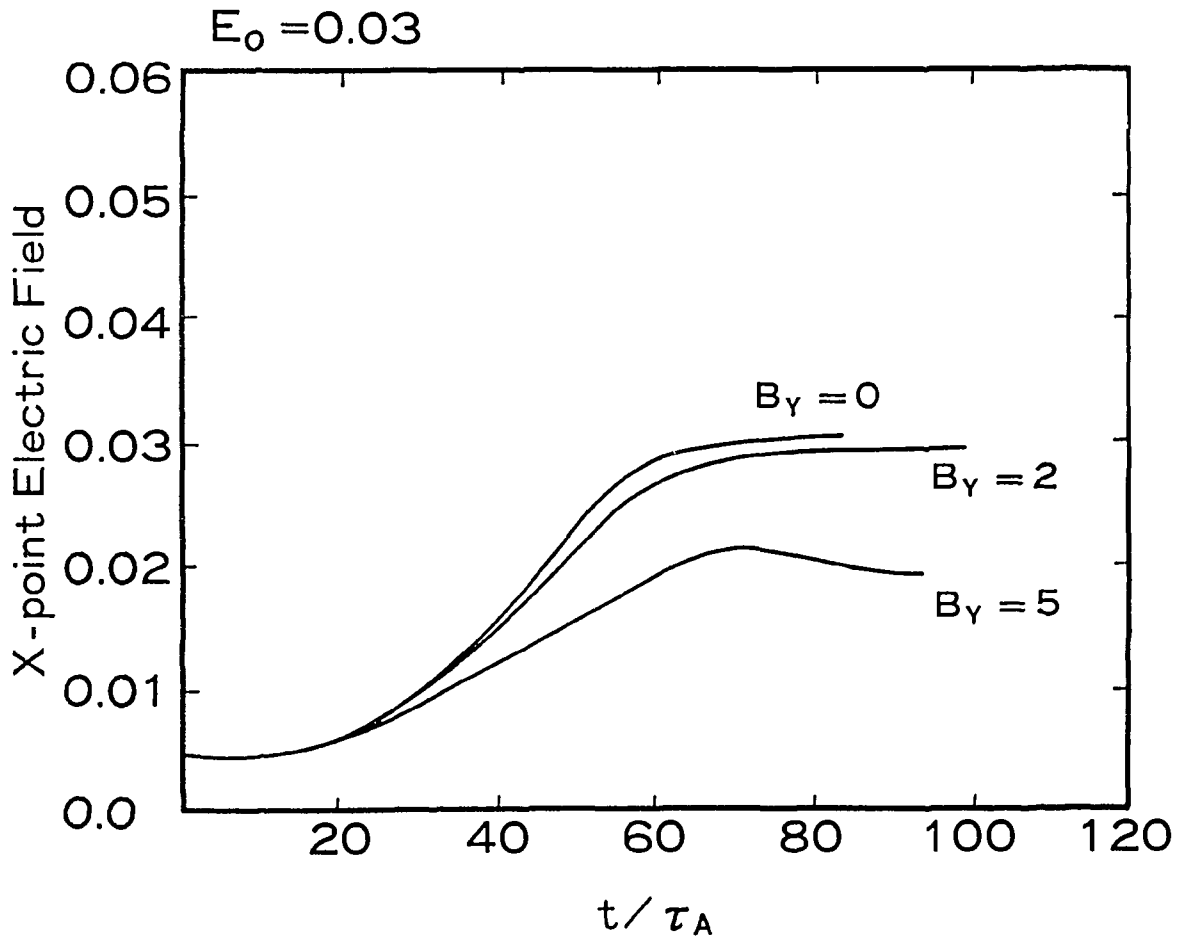
E_o =0.03
0.06
0.05
0.04
0.03
0.02
0.01
0.0
X-point Electric Field
B_Y = 0
B_Y = 2
B_Y = 5
20
40
60
80
100
120
t/τ_A

Figure 11-(a)

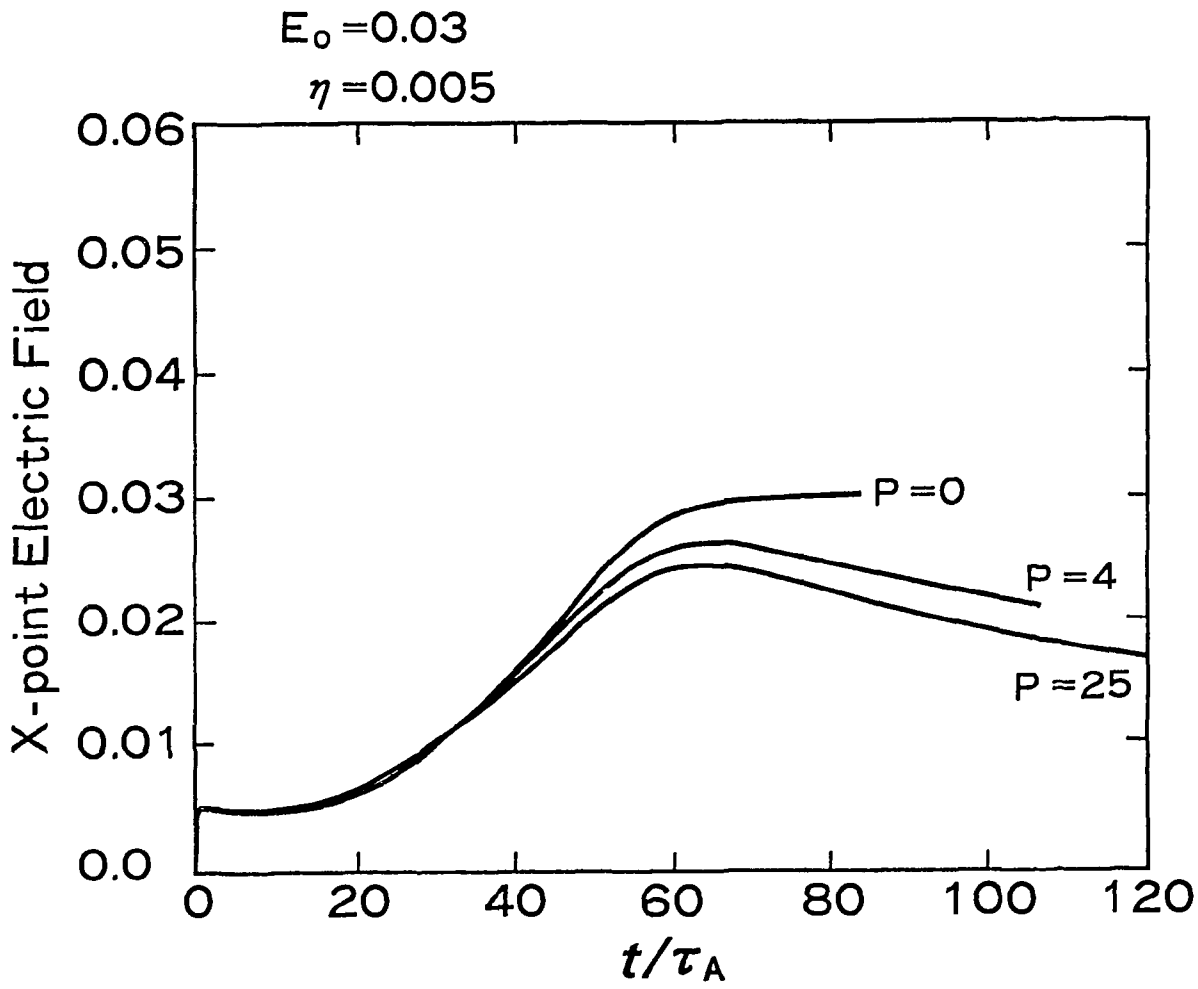
E_o =0.03
η =0.005
X-point Electric Field
0.06
0.05
0.04
0.03
0.02
0.01
0.0
0
20
40
60
80
100
120
t/τ_A
P =0
P =4
P =25

Figure 11-(b)

Recent Issues of NIFS Series

NIFS-48 T.Seki, R.Kumazawa, Y.Takase, A.Fukuyama, T.Watari, A.Ando, Y.Oka, O.Kaneko, K.Adati, R.Akiyama, R.Ando, T.Aoki, Y.Hamada, S.Hidekuma, S.Hirokura, K.Ida, K.Itoh, S.-I.Itoh, E.Kako, A. Karita, K.Kawahata, T.Kawamoto, Y.Kawasumi, S.Kitagawa, Y.Kitoh, M.Kojima, T.Kuroda, K.Masai, S.Morita, K.Narihara, Y.Ogawa, K.Ohkubo, S.Okajima, T.Ozaki, M.Sakamoto, M.Sasao, K.Sato, K.N.Sato, F.Shinbo, H.Takahashi, S.Tanahashi, Y.Taniguchi, K.Toi and T.Tsuzuki, *Application of Intermediate Frequency Range Fast Wave to JIPP T-IIU Plasma*; Sep.1990

NIFS-49 A.Kageyama, K.Watanabe and T.Sato, *Global Simulation of the Magnetosphere with a Long Tail: The Formation and Ejection of Plasmoids*; Sep.1990

NIFS-50 S.Koide, *3-Dimensional Simulation of Dynamo Effect of Reversed Field Pinch*; Sep. 1990

NIFS-51 O.Motojima, K. Akaishi, M.Asao, K.Fujii, J.Fujita, T.Hino, Y.Hamada, H.Kaneko, S.Kitagawa, Y.Kubota, T.Kuroda, T.Mito, S.Morimoto, N.Noda, Y.Ogawa, I.Ohtake, N.Ohyabu, A.Sagara, T. Satow, K.Takahata, M.Takeo, S.Tanahashi, T.Tsuzuki, S.Yamada, J.Yamamoto, K.Yamazaki, N.Yanagi, H.Yonezu, M.Fujiwara, A.Iiyoshi and LHD Design Group, *Engineering Design Study of Superconducting Large Helical Device*; Sep. 1990

NIFS-52 T.Sato, R.Horiuchi, K. Watanabe, T. Hayashi and K.Kusano, *Self-Organizing Magnetohydrodynamic Plasma*; Sep. 1990

NIFS-53 M.Okamoto and N.Nakajima, *Bootstrap Currents in Stellarators and Tokamaks*; Sep. 1990

NIFS-54 K.Itoh and S.-I.Itoh, *Peaked-Density Profile Mode and Improved Confinement in Helical Systems*; Oct. 1990

NIFS-55 Y.Ueda, T.Enomoto and H.B.Stewart, *Chaotic Transients and Fractal Structures Governing Coupled Swing Dynamics*; Oct. 1990

NIFS-56 H.B.Stewart and Y.Ueda, *Catastrophes with Indeterminate Outcome*; Oct. 1990

NIFS-57 S.-I.Itoh, H.Maeda and Y.Miura, *Improved Modes and the Evaluation of Confinement Improvement*; Oct. 1990

NIFS-58 H.Maeda and S.-I.Itoh, *The Significance of Medium- or Small-size Devices in Fusion Research*; Oct. 1990

NIFS-59 A.Fukuyama, S.-I.Itoh, K.Itoh, K.Hamamatsu, V.S.Chan, S.C.Chiu, R.L.Miller and T.Ohkawa, *Nonresonant Current Drive by RF Helicity Injection*; Oct. 1990

NIFS-60 K.Ida, H.Yamada, H.Iguchi, S.Hidekuma, H.Sanuki, K.Yamazaki and CHS Group, *Electric Field Profile of CHS Heliotron/Torsatron Plasma with Tangential Neutral Beam Injection*; Oct. 1990

NIFS-61 T.Yabe and H.Hoshino, *Two- and Three-Dimensional Behavior of Rayleigh-Taylor and Kelvin-Helmholz Instabilities*; Oct. 1990

NIFS-62 H.B. Stewart, *Application of Fixed Point Theory to Chaotic Attractors of Forced Oscillators*; Nov. 1990

NIFS-63 K.Konn., M.Mituhashi, Yoshi H.Ichikawa,*Soliton on Thin Vortex Filament;* Dec. 1990

NIFS-64 K.Itoh, S.-I.Itoh and A.Fukuyama,*Impact of Improved Confinement on Fusion Research;* Dec. 1990

NIFS -65 A.Fukuyama, S.-I.Itoh and K. Itoh,*A Consistency Analysis on the Tokamak Reactor Plasmas;* Dec. 1990

NIFS-66 K.Itoh, H. Sanuki, S.-I. Itoh and K. Tani,*Effect of Radial Electric Field on α-Particle Loss in Tokamaks;* Dec. 1990

NIFS-67 K.Sato,and F.Miyawaki,*Effects of a Nonuniform Open Magnetic Field on the Plasma Presheath*; Jan.1991

NIFS-68 K.Itoh and S.-I.Itoh,*On Relation between Local Transport Coefficient and Global Confinement Scaling Law;* Jan. 1991

NIFS-69 T.Kato, K.Masai, T.Fujimoto,F.Koike, E.Källne, E.S.Marmar and J.E.Rice,*He-like Spectra Through Charge Exchange Processes in Tokamak Plasmas;* Jan.1991

NIFS-70 K. Ida, H. Yamada, H. Iguchi, K. Itoh and CHS Group, *Observation of Parallel Viscosity in the CHS Heliotron/Torsatron* ; Jan.1991

NIFS-71 H. Kaneko, *Spectral Analysis of the Heliotron Field with the Toroidal Harmonic Function in a Study of the Structure of Built-in Divertor* ; Jan. 1991

NIFS-72 S. -I. Itoh, H. Sanuki and K. Itoh, *Effect of Electric Field Inhomogeneities on Drift Wave Instabilities and Anomalous Transport* ; Jan. 1991

NIFS-73 Y.Nomura, Yoshi.H.Ichikawa and W.Horton, *Stabilities of Regular Motion in the Relativistic Standard Map*; Feb. 1991

NIFS-74 T.Yamagishi, *Electrostatic Drift Mode in Toroidal Plasma with Minority Energetic Particles,* Feb. 1991

NIFS-75 T.Yamagishi, *Effect of Energetic Particle Distribution on Bounce Resonance Excitation of the Ideal Ballooning Mode,* Feb. 1991

NIFS-76 T.Hayashi, A.Tadei, N.Ohyabu and T.Sato, *Suppression of Magnetic Surface Breading by Simple Extra Coils in Finite Beta Equilibrium of Helical System;* Feb. 1991

NIFS-77 N. Ohyabu, *High Temperature Divertor Plasma Operation*; Feb. 1991

NIFS-78 K.Kusano, T. Tamano and T. Sato, *Simulation Study of Toroidal Phase-Locking Mechanism in Reversed-Field Pinch Plasma*; Feb. 1991

NIFS-79 K. Nagasaki, K. Itoh and S. -I. Itoh, *Model of Divertor Biasing and Control of Scrape-off Layer and Divertor Plasmas*; Feb. 1991

NIFS-80 K. Nagasaki and K. Itoh, *Decay Process of a Magnetic Island by Forced Reconnection*; Mar. 1991

NIFS-81 K. Takahata, N. Yanagi, T. Mito, J. Yamamoto, O.Motojima and LHDDesign Group, K. Nakamoto, S. Mizukami, K. Kitamura, Y. Wachi, H. Shinohara, K. Yamamoto, M. Shibui, T. Uchida and K. Nakayama, *Design and Fabrication of Forced-Flow Coils as R&D Program for Large Helical Device*; Mar. 1991

NIFS-82 T. Aoki and T. Yabe, *Multi-dimensional Cubic Interpolation for ICF Hydrodynamics Simulation*; Apr. 1991

NIFS-83 K. Ida, S.-I. Itoh, K. Itoh, S. Hidekuma, Y. Miura, H. Kawashima, M. Mori, T. Matsuda, N. Suzuki, H. Tamai, T.Yamauchi and JFT-2M Group, *Density Peaking in the JFT-2M Tokamak Plasma with Counter Neutral Beam Injection* ; May 1991

NIFS-84 A. Iiyoshi, *Development of the Stellarator/Heliotron Research*; May 1991

NIFS-85 Y. Okabe, M. Sasao, H. Yamaoka, M. Wada and J. Fujita, *Dependence of Au^- Production upon the Target Work Function in a Plasma-Sputter-Type Negative Ion Source;* May 1991

NIFS-86 N. Nakajima and M. Okamoto, *Geometrical Effects of the Magnetic Field on the Neoclassical Flow, Current and Rotation in General Toroidal Systems*; May 1991

NIFS-87 S. -I. Itoh, K. Itoh, A. Fukuyama, Y. Miura and JFT-2M Group, *ELMy-H mode as Limit Cycle and Chaotic Oscillations in Tokamak Plasmas;* May 1991

NIFS-88 N.Matsunami and K.Kitoh, *High Resolution Spectroscopy of H^+ Energy Loss in Thin Carbon Film;* May 1991

NIFS-89 H. Sugama, N. Nakajima and M.Wakatani, *Nonlinear Behavior of Multiple-Helicity Resistive Interchange Modes near Marginally Stable States;* May 1991

NIFS-90 H. Hojo and T.Hatori, *Radial Transport Induced by Rotating RF Fields and Breakdown of Intrinsic Ambipolarity in a Magnetic Mirror*; May 1991

NIFS-91 M. Tanaka, S. Murakami, H. Takamaru and T.Sato, *Macroscale Implicit, Electromagnetic Particle Simulation of Inhomogeneous and Magnetized Plasmas in Multi-Dimensions;* May 1991

NIFS-92 S. - I. Itoh, *H-mode Physics, -Experimental Observations and Model Theories-, Lecture Notes, Spring College on Plasma Physics, May 27 - June 21 1991 at International Centre for Theoretical Physics (IAEA UNESCO) Trieste, Italy ;* Jun. 1991

NIFS-93 Y. Miura, K. Itoh, S. - I. Itoh, T. Takizuka, H. Tamai, T. Matsuda, N. Suzuki, M. Mori, H. Maeda and O. Kardaun, *Geometric Dependence of the Scaling Law on the Energy Confinement Time in H-mode Discharges;* Jun. 1991

NIFS-94 H. Sanuki, K. Itoh, K. Ida and S. - I. Itoh, *On Radial Electric Field Structure in CHS Torsatron / Heliotron;* Jun. 1991

NIFS-95 K. Itoh, H. Sanuki and S. - I. Itoh, *Influence of Fast Ion Loss on Radial Electric Field in Wendelstein VII-A Stellarator;* Jun. 1991

NIFS-96 S. - I. Itoh, K. Itoh, A. Fukuyama, *ELMy-H mode as Limit Cycle and Chaotic Oscillations in Tokamak Plasmas;* Jun. 1991

NIFS-97 K. Itoh, S. - I. Itoh, H. Sanuki, A. Fukuyama, *An H-mode-Like Bifurcation in Core Plasma of Stellarators;* Jun. 1991

NIFS-98 H. Hojo, T. Watanabe, M. Inutake, M. Ichimura and S. Miyoshi, *Axial Pressure Profile Effects on Flute Interchange Stability in the Tandem Mirror GAMMA 10;* Jun. 1991

NIFS-99 A. Usadi, A. Kageyama, K. Watanabe and T. Sato, *A Global Simulation of the Magnetosphere with a Long Tail : Southward and Northward IMF;* Jun. 1991

NIFS-100 H. Hojo, T. Ogawa and M. Kono, *Fluid Description of Ponderomotive Force Compatible with the Kinetic One in a Warm Plasma* ; July 1991

NIFS-101 H. Momota, A. Ishida, Y. Kohzaki, G. H. Miley, S. Ohi, M. Ohnishi K. Yoshikawa, K. Sato, L. C. Steinhauer, Y. Tomita and M. Tuszewski *Conceptual Design of D-^{3}He FRC Reactor "ARTEMIS"* ; July 1991

NIFS-102 N. Nakajima and M. Okamoto, *Rotations of Bulk Ions and Impurities in Non-Axisymmetric Toroidal Systems* ; July 1991

NIFS-103 A. J. Lichtenberg, K. Itoh, S. - I. Itoh and A. Fukuyama, *The Role of Stochasticity in Sawtooth Oscillation* ; Aug. 1991

NIFS-104 K. Yamazaki, T. Amano, *Plasma Transport Simulation Modeling for Helical Confinement Systems;* Aug. 1991